Perfect Higher-Order Poincaré Sphere Beams from Digitalized Geometric Phases

Ran Xu,[1,2] Peng Chen,[1] Jie Tang,[1] Wei Duan,[1] Shi-Jun Ge,[1,2] Ling-Ling Ma,[1] Run-Xin Wu,[3] Wei Hu,[1,2,*] and Yan-Qing Lu[1,†]

[1]*National Laboratory of Solid State Microstructures, Collaborative Innovation Center of Advanced Microstructures, and College of Engineering and Applied Sciences, Nanjing University, Nanjing 210093, China*
[2]*Institute for Smart Liquid Crystals, JITRI, Changshu 215500, China*
[3]*Nanjing Foreign Languages School, Nanjing 210008, China*

(Received 8 February 2018; revised manuscript received 9 May 2018; published 27 September 2018)

For a conventional higher-order Poincaré (HOP) sphere beam that generalizes optical vortices and vector beams, its donutlike intensity profile varies significantly with topological charges, which is undesirable for many applications in optical manipulations and communications. Recently, the perfect optical vortex and perfect vector beam have been reported to provide a solution. Until now, this strategy has not been extended to the whole HOP sphere. In this work, the concept of a perfect HOP sphere is proposed for the first time and realized by digitalizing the spiral geometric phase with specific structures of circular Dammann gratings (CDGs), which are demonstrated in liquid crystals through dynamic photo-patterning. Via selecting the incident spin, any point on the perfect HOP sphere can be obtained. Properly programming CDGs makes both single- and multi-ringed perfect HOP sphere beams achievable with merits of high efficiency and uniform energy distribution. All experimental results are qualitatively consistent with the theoretical calculations. This integrated liquid crystal device paves the way for perfect optical angular momentum manipulation and facilitates numerous cutting-edge applications.

DOI: 10.1103/PhysRevApplied.10.034061

I. INTRODUCTION

The higher-order Poincaré (HOP) sphere generalizes optical vortices (OVs) and vector beams (VBs), and vividly describes their higher-order polarization states [1–5]. Compared with a traditional Poincaré sphere whose poles indicate two opposite spin angular momentum (SAM) eigenstates, the poles of a HOP sphere represent orthogonally circularly polarized OVs. These two eigenstates are featured by helical phase-fronts ($e^{\pm im\phi}$) and orbital angular momentums (OAMs, $\pm m\hbar$, m is the topological charge) [6,7]. Each point on the HOP sphere is their linear superposition. The equator especially indicates VBs featured by space-variant linear polarizations [8–10]. The HOP sphere incorporates SAM and OAM, thus extending to a higher-dimension angular momentum and adding a new degree of freedom to the manipulation of light [2,11]. Over the past few years, HOP sphere beams have attracted extensive attention in optical trapping, super-resolution imaging, and quantum informatics [8,12]. In particular, these transverse spatial modes can drastically enhance the capacity of optical communication systems via mode-division multiplexing [13].

For a conventional OV, the phase singularity in the beam center results in a donutlike intensity distribution. Normally, its ring radius increases proportionally with $|m|$ [12]. This is undesirable for some practical applications, for instance, the simultaneous coupling and copropagation of multiple OVs in multiplexing communications, and the minimized high-speed rotators in optical manipulation. Perfect optical vortex (POV) supplies a solution, permitting the topological-charge-independent annular intensity profile and beam divergence [14–16]. More recently, the perfect vector beam (PVB) was proposed to address a similar issue in traditional VBs [17]. To date, several strategies, such as spatial light modulators (SLMs) [18–20] and plasmonic metasurfaces [21,22], have been developed for generating POVs/PVBs. Unfortunately, the former suffers from complex optical setup and low efficiency, while the latter is compact but still faces an issue of insufficient efficiency. Until now, only typical POVs/PVBs have been presented. If one can extend this concept to the whole HOP sphere via a simple device, the manipulation of higher-dimension angular momentum of light can be fully achieved, upgrading wide applications from optical manipulation [23] and microscopy imaging [24] to laser fabrication [25].

In this work, the concept of a perfect HOP sphere beam is proposed and demonstrated in photo-patterned liquid crystals (LCs) by digitalizing the spiral geometric phase of q plates with circular Dammann gratings (CDGs). This compact LC device brings traditional POV to a new level with an arbitrary m, spatial polarization, and

*huwei@nju.edu.cn
†yqlu@nju.edu.cn

energy distribution. Thanks to the fixed intensity profile and programmable diffraction orders determined by CDG parameters, both single- and multi-ringed HOP sphere beams are highly efficiently generated with a normalized annular radius and uniform energy distribution. Each point on the perfect HOP sphere can be directly obtained via selecting the incident spin state. Such versatile LC devices supply an exacting technique for perfect total angular momentum processing.

II. DESIGN AND PRINCIPLE

The CDG [26,27] can be regarded as a polar transformation of the conventional Dammann grating [28–30]. It is composed of radially periodic concentric rings imprinted with alternative binary phases (usually 0 and π) [31–33], whose transmission function can be represented as

$$T(r) = \exp[i\varphi_{\mathrm{CDG}}(r)] = \sum_{n=0}^{+\infty} C_n \exp(i2\pi rn/\Lambda), \qquad (1)$$

where $\varphi_{\mathrm{CDG}}(r)$ is the phase profile of a CDG, r is the polar radius, Λ is the period, and C_n is the coefficient of the nth diffracted ring. The power ratio of the nth order to the total can be expressed as $|C_n|^2$. By optimizing the number and values of phase transition points, the incident light can be highly efficiently diffracted into several desired concentric rings with uniform energy distribution [26,27,31]. Thus, the energies of different rings are proportional to their respective sizes.

Here, the CDG is adopted to digitalize the spiral geometric phase of a q plate [34,35]. The encoded CDG is a specific binary phase pattern, just like digital information coding (binary code: 0 and 1). Therefore, we call such a process of encoding CDG into the spiral geometric phase "*digitalizing*." Compared with the dynamic phase that arises from optical path differences, the geometric phase is associated with the space-variant manipulation of the polarization state and depends only on the geometrical characteristics [36]. Usually, its magnitude is proportional to the orientation angle of the local optical axis and has a spin-dependent sign. By encoding the CDG into the q plate, a circular-Dammann-q-plate (CDQP) can be obtained. Its optical axis orientation α follows:

$$\alpha = \frac{1}{2} m\phi + \frac{\varphi_{\mathrm{CDG}}}{2}, \qquad (2)$$

where $\phi(x,y) = \arctan(y/x)$ indicates the azimuthal angle. Figure 1 shows optical axis distributions of a first-order CDG with a single normalized phase transition point ($r_1 = 0.5$), a q plate with $m = 1$, and the corresponding integrated CDQP, respectively. The gray color variation indicates the space-variant optical axis, which is further vividly shown by the purple sticks.

Jones matrix calculation [37] is employed to analyze the diffraction resulting from the optical spin-orbit interaction. For an arbitrary incident beam, the polarization state can be expressed as

$$|u_{\mathrm{in}}\rangle = \cos\left(\frac{\Theta}{2}\right) e^{-i(\Phi/2)}|L\rangle + \sin\left(\frac{\Theta}{2}\right) e^{i(\Phi/2)}|R\rangle. \qquad (3)$$

$|u_{\mathrm{in}}\rangle$ is an arbitrary point on a traditional Poincaré sphere, for which the spherical coordinate is (Θ, Φ). $|L\rangle = \frac{1}{\sqrt{2}}\begin{pmatrix}1\\ i\end{pmatrix}$ and $|R\rangle = \frac{1}{\sqrt{2}}\begin{pmatrix}1\\ -i\end{pmatrix}$ represent the left and right circular polarization (LCP/RCP), respectively. Considering a half-wave plate with α as its optical axis distribution, the Jones matrix is

$$\mathbf{J} = \begin{bmatrix}\cos(2\alpha) & \sin(2\alpha)\\ \sin(2\alpha) & -\cos(2\alpha)\end{bmatrix}. \qquad (4)$$

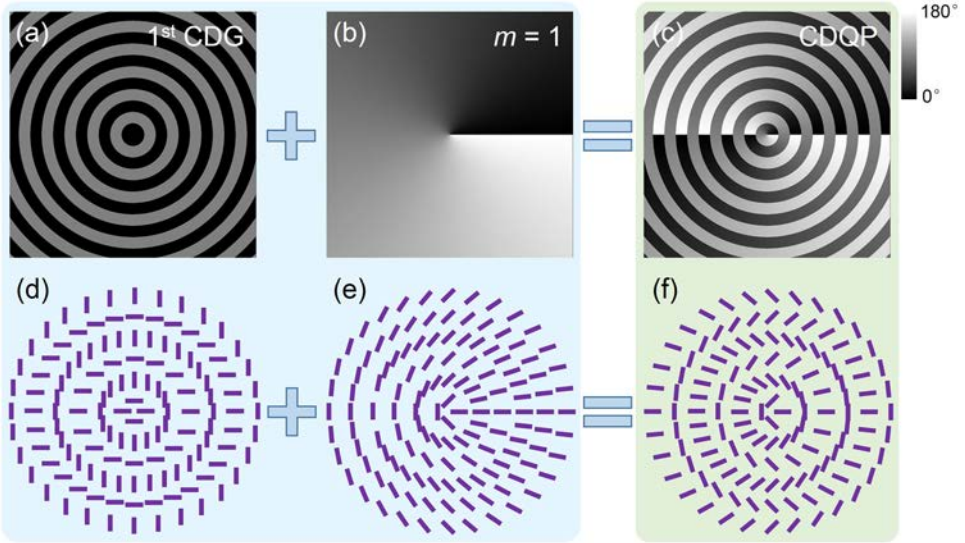

FIG. 1. Optical axis distributions of (a),(d) a first-order CDG, (b),(e) a q plate with $m = 1$, and (c),(f) the integrated CDQP. The color variation from black to white corresponds to the axis varying from 0° to 180°, and the purple sticks represent the local optical axis orientations.

Substituting Eq. (2), the output light from a CDQP ($|u_{\text{out}}\rangle = \mathbf{J}|u_{\text{in}}\rangle$) is transformed to

$$\begin{aligned}|u_{\text{out}}\rangle &= \cos\left(\frac{\Theta}{2}\right) e^{-i(\Phi/2)}|R\rangle e^{i2\alpha} \\ &\quad + \sin\left(\frac{\Theta}{2}\right) e^{i(\Phi/2)}|L\rangle e^{-i2\alpha} \\ &= \left[\cos\left(\frac{\Theta}{2}\right) e^{-i(\Phi/2)}|R_m\rangle \right. \\ &\quad \left. + \sin\left(\frac{\Theta}{2}\right) e^{i(\Phi/2)}|L_{\bar{m}}\rangle\right] e^{i\varphi_{\text{CDG}}} \\ &= \sum_{n=0}^{+\infty} C_n \exp(i2\pi rn/\Lambda)|u_m\rangle. \end{aligned} \tag{5}$$

$\pm 2\alpha$ is the geometric phase. $|R_m\rangle = |R\rangle e^{im\phi}$ and $|L_{\bar{m}}\rangle = |L\rangle e^{-im\phi}$ are the two poles of the HOP sphere, and their linear superposition $|u_m\rangle = \cos(\Theta/2)e^{-i(\Phi/2)}|R_m\rangle + \sin(\Theta/2)e^{i(\Phi/2)}|L_{\bar{m}}\rangle$ depicts all points on the HOP sphere [2,3]. Accordingly, OV, VB, and other intermediate states can be obtained by controlling the incident polarization. Moreover, the CDG term contributes to the uniformly distributed concentric ring(s). For a fixed incident wavelength and diffraction distance, the radius of a desired ring is determined only by Λ, thus it is definitely independent of m. Therefore, a single- or multi-ringed "perfect HOP sphere beam" can be conveniently created with a spin-controlled state.

Such a CDQP can be demonstrated in inhomogeneous anisotropic media, among which LC is most promising for its pronounced high optical anisotropy/transparency over a

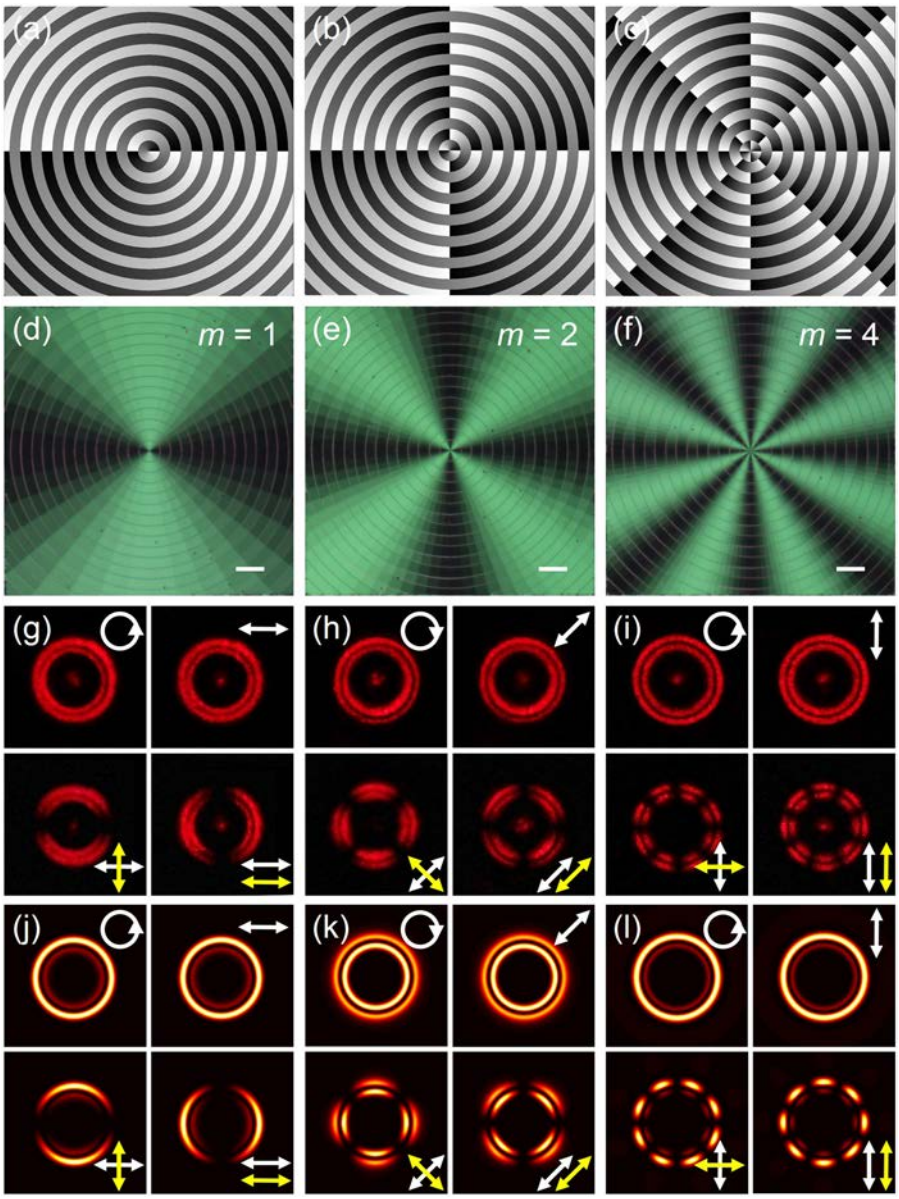

FIG. 2. The designed optical axis distributions, micrographs under a polarized optical microscope, experimental and theoretically calculated diffraction patterns with different incident polarization of three first-order CDQPs with (a),(d),(g),(j) $m = 1$, (b),(e),(h),(k) $m = 2$, and (c),(f),(i),(l) $m = 4$, respectively. (g)–(i) show experimental results while (j)–(l) show corresponding simulations. All scale bars are 100 μm. The white and yellow arrows indicate the polarization states of incident light and the direction of the analyzer, respectively.

wide electromagnetic spectrum and reconfigurable space-variant director (i.e., local optical axis) orientation. Moreover, the electro-optical tunability of LC makes it possible to dynamically switch and operate at different wavelengths [30]. When the induced phase retardation satisfies the half-wave condition, which means $\Gamma = [(2\pi(n_{\text{eff}} - n_o)d)/\lambda] = (2a+1)\pi$ (d: LC cell gap, λ: incident wavelength, n_{eff}: effective extraordinary refractive index, a: an integer), the perfect HOP sphere beam can be generated with maximum efficiency (ON state). While for $\Gamma = 2a\pi$, the diffraction will be suppressed (OFF state).

III. RESULTS AND DISCUSSION

To accurately transfer the designed optical axis distributions, LC photoalignment, which is particularly suitable for high-quality and high-resolution multi-domain LC alignment [38,39], is adopted. Here, a polarization-sensitive sulfonic azo-dye SD1 is used as the photoalignment agent. Under linearly polarized UV exposure, the SD1 molecules tend to reorient their absorption oscillators perpendicular to the incident polarization [40]. The orientation of SD1 will spread to adjacent LC molecules via intermolecular interactions and thus guide the LC directors. Two pieces of indium-tin-oxide glass substrates spin-coated with SD1 are assembled with 6.0-μm spacers and sealed with epoxy glue to configure the cell. Then, a multi-step partly-overlapping exposure process is performed to carry out the desired structure through a dynamic micro-lithography system [4,41]. Afterward, filling the cell with nematic LC E7 yields the proposed CDQPs.

Figure 2(d) shows the micrograph of the first-order CDQP with $m = 1$, whose theoretical optical axis distribution is depicted in Fig. 2(a) [i.e., Fig. 1(c)]. The continuous change of the brightness is due to the varying of LC directors. The bright domains correspond to regions with LC directors around 45° with respect to the polarizer or analyzer of the microscope, whereas the dark domains correspond to regions with LC directors approximately parallel to the polarizer or analyzer. Compared with the q plate with $m = 1$, concentric-circle-like disclinations are observed, which are caused by the 90° shift of LC directors at the boundaries of adjacent domains. All of these indicate that the designed optical axis distribution is faithfully imprinted. CDQPs with $m = 2$ and $m = 4$ are also presented. They are featured by denser brightness alternation and are capable of higher-order perfect HOP sphere beams generation.

Figure 3(a) illustrates the optical setup for generating and analyzing perfect HOP sphere beams. A quarter-wave plate (QWP) is utilized to convert the linearly polarized laser beam ($\lambda = 632.8$ nm) into circular polarization. Handedness conversion is realized via properly rotating the QWP. Different linear polarization is selected via inserting and rotating a polarizer (P1). The second polarizer (P2) is

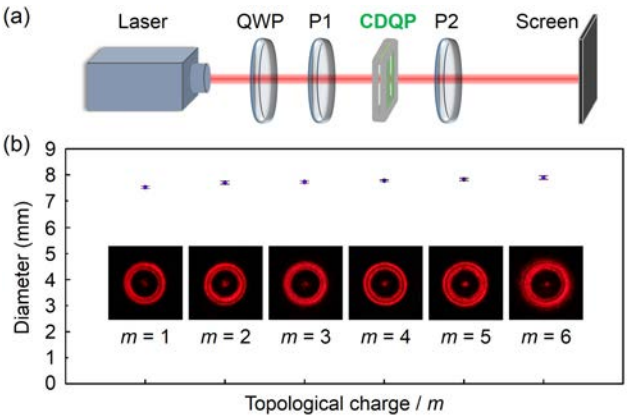

FIG. 3. (a) Optical setup for generating and analyzing perfect HOP sphere beams. QWP: quarter-wave plate, P1: polarizer, P2: analyzer. (b) The dependence of the ring diameter on the topological charge m. Insets: the diffraction patterns with $m = 1$–6.

adopted to analyze the output polarization. Consequently, any special cases corresponding to the poles or equator of a perfect HOP sphere, which are commonly used for the demonstration of HOP sphere beams, are tested and presented in Figs. 2–4. Theoretically, to cover all the points on the HOP sphere, arbitrary incident polarization should be realized. An extra QWP should be inserted between P1 and CDQP. It needs to be noted that in this case, the combination of a half-wave plate and a QWP can realize the same function more compactly and energy efficiently. The resultant perfect HOP sphere beams project on the screen and are captured by a camera. A voltage of 2.5 V is applied to keep the half-wave condition. The far field diffraction patterns with different incident polarizations of the sample in Fig. 2(d) are shown in Fig. 2(g). When $|u_{\text{in}}\rangle = |R\rangle$, one annular ring pattern can be clearly observed with LCP and $m = -1$, i.e., the point on the south pole of the HOP sphere ($|L_{-1}\rangle$). While for $|u_{\text{in}}\rangle = |L\rangle$, $|R_{+1}\rangle$ is generated, corresponding to the north pole. For linear incident polarization, the horizontal polarization ($|u_{\text{in}}\rangle = (1/\sqrt{2})[|L\rangle + |R\rangle]$) for example, a radially polarized VB $\{(1/\sqrt{2})[|R_{+1}\rangle + |L_{-1}\rangle]\}$ is obtained, with corresponding lobed structures parallel to the orientation of the analyzer. These experimental results qualitatively match the theoretical ones shown in Fig. 2(j). Although only two special cases are presented here, other HOP sphere beams can be easily realized via controlling the incident spin. Cases for the other two LC CDQPs with large m are also exhibited in Figs. 2(h) and 2(i), which are in good qualitative agreement with the calculated results in Figs. 2(k) and 2(l), respectively, where the number of petals is equal to $2m$ in VB analyzing.

In contrast to conventional OVs from q plates, all the generated ring patterns are almost identical. To verify the "perfect" property of the resultant HOP sphere beams, the dependence of the ring diameter on the

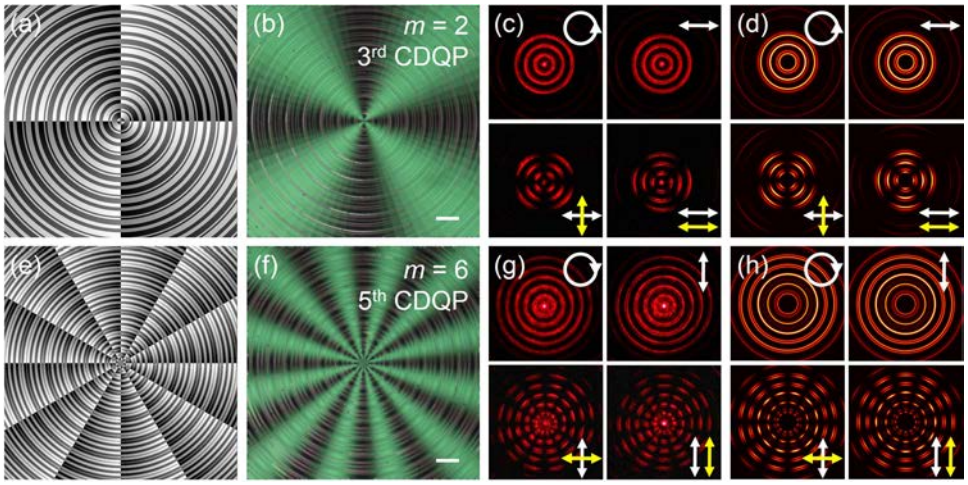

FIG. 4. The designed optical axis distributions, micrographs, experimental, and calculated diffraction patterns with different incident polarization of (a)–(d) the third-order CDQP with $m = 2$, and (e)–(h) the fifth-order CDQP with $m = 6$, respectively. (c),(g) show experimental results while (d),(h) show corresponding simulations. All scale bars are 100 μm. The white and yellow arrows indicate the polarization states of incident light and the direction of the analyzer, respectively.

topological charge is investigated as exhibited in Fig. 3(b). The incident is circular polarization and the diffraction distance is fixed. The annular patterns with $m = 1$–6 are inserted for a vivid comparison. The measured diameter satisfies the diffraction equation and is nearly invariable with m. Similar phenomena are observed in other HOP sphere beams. The diffraction efficiency (η), defined as the power ratio of the desired ring to the total output, is detected as well. For the first-order LC CDQP here, the average η is 78.6%, approaching the theoretical value of 81% [31]. All experimental results are consistent with the theoretical prediction, verifying the highly efficient generation of perfect HOP sphere beams.

Thanks to the unique feature of CDGs, not only single-ringed perfect HOP sphere beams are expected. Via properly designing the phase transition points of the CDG, multi-ringed patterns can be obtained. Figures 4(a) and 4(e) present two CDQPs with $m = 2$ and $m = 6$, which are digitalized by the third- and fifth-order CDGs, respectively. The corresponding micrographs are shown in Figs. 4(b) and 4(f). They feature denser concentric-circle-like disclinations, resulting from more normalized phase transition points within each period [31]. Three-ringed and five-ringed perfect HOP sphere beams are generated in a uniform energy distribution [Figs. 4(c) and 4(g)]. Special points of $(1/\sqrt{2})[|R_{+2}\rangle + |L_{-2}\rangle]$ and $(i/\sqrt{2})[-|R_{+6}\rangle + |L_{-6}\rangle]$ are presented with hierarchical lobed structures after transmission through an analyzer. As expected, η of different rings are proportional to their radii, while the total efficiency is consistent with the theoretical value. Compared to the calculated diffraction results shown in Figs. 4(d) and 4(h), the stronger zeroth order and slight inhomogeneity of different rings are attributed to the fabrication deviation of such an ultra-fine structure, which could be improved with a higher-resolution fabrication [42].

Actually, the number of rings could be freely designed via programming CDG parameters. These multi-ringed perfect HOP sphere beams are created for the first time, which may inspire applications in parallel microstructure fabrications [25,43], multiple optical tweezers, and space-integrated mode-division multiplexing optical communications. The topological charge of a perfect HOP sphere can be arbitrarily designed by the geometric phase. Integral, fractional m, and even more complex modes [30,35] can be expected. Additionally, LC electro-optical tunability makes the CDQP wavelength tolerant. Introducing special LC materials may produce other fascinating functionalities [41]. Additional techniques (such as laser direct writing [42], photoalignment with photonic metamasks [44]), and even artificial anisotropic media (such as plasmonic metasurfaces [21,22]) can also be adopted to demonstrate the proposed perfect HOP sphere.

IV. CONCLUSION

In summary, the concept of perfect HOP sphere is proposed and realized by digitalizing q plates with CDGs. Via properly programming CDGs and spiral geometric phases, single- and multi-ringed perfect HOP sphere beams with arbitrary topological charges are achievable. Each point on a perfect HOP sphere can be obtained by controlling the incident polarization. Moreover, this versatile LC device exhibits the merits of high efficiency, uniform energy distribution, high quality, simple configuration, and broadband tolerance. This work extends the understanding on geometric phase engineering and may provide new opportunities for angular momentum lightened applications.

ACKNOWLEDGMENTS

This work was supported by the National Key Research and Development Program of China (Grant No. 2017YFA0303700), the National Natural Science Foundation of China (NSFC) (Grants No. 61575093, No. 61490714, and No. 61435008), the Fundamental Research Funds for the Central Universities, the Distinguished Young Scholars Fund of Jiangsu Province (Grant No. BK20180004), and the Scientific Research Foundation

of Graduate School of Nanjing University (Grant No. 2017ZDL06).

R.X. and P.C. contributed equally to this work.

[1] G. Milione, H. Sztul, D. Nolan, and R. Alfano, Higher-order Poincaré Sphere, Stokes Parameters, and the Angular Momentum of Light, Phys. Rev. Lett. **107**, 053601 (2011).

[2] G. Milione, S. Evans, D. Nolan, and R. Alfano, Higher Order Pancharatnam-Berry Phase and the Angular Momentum of Light, Phys. Rev. Lett. **108**, 190401 (2012).

[3] D. Naidoo, F. S. Roux, A. Dudley, I. Litvin, B. Piccirillo, L. Marrucci, and A. Forbes, Controlled generation of higher-order Poincaré sphere beams from a laser, Nat. Photonics **10**, 327 (2016).

[4] P. Chen, S. J. Ge, W. Duan, B. Y. Wei, G. X. Cui, W. Hu, and Y. Q. Lu, Digitalized geometric phases for parallel optical spin and orbital angular momentum encoding, ACS Photonics **4**, 1333 (2017).

[5] R. C. Devlin, A. Ambrosio, N. A. Rubin, J. B. Mueller, and F. Capasso, Arbitrary spin-to-orbital angular momentum conversion of light, Science **358**, 896 (2017).

[6] L. Allen, M. W. Beijersbergen, R. Spreeuw, and J. Woerdman, Orbital angular momentum of light and the transformation of Laguerre-Gaussian laser modes, Phys. Rev. A **45**, 8185 (1992).

[7] K. Huang, H. Liu, S. Restuccia, M. Q. Mehmood, S. Mei, D. Giovannini, A. Danner, M. J. Padgett, J. Teng, and C. W. Qiu, Spiniform phase-encoded metagratings entangling arbitrary rational-order orbital angular momentum, Light Sci. Appl. **7**, e17156 (2018).

[8] Q. Zhan, Cylindrical vector beams: from mathematical concepts to applications, Adv. Opt. Photonics **1**, 1 (2009).

[9] F. Cardano, E. Karimi, S. Slussarenko, L. Marrucci, C. de Lisio, and E. Santamato, Polarization pattern of vector vortex beams generated by q-plates with different topological charges, Appl. Opt. **51**, C1 (2012).

[10] G. G. Liu, Y. H. Lee, Y. Huang, Z. Zhu, G. Tan, M. Q. Cai, P. P. Li, D. Wang, Y. Li, S. Pang, C. Tu, S. T. Wu, and H. T. Wang, Dielectric broadband meta-vector-polarizers based on nematic liquid crystal, APL Photonics **2**, 126102 (2017).

[11] F. Yue, D. Wen, C. Zhang, B. D. Gerardot, W. Wang, S. Zhang, and X. Chen, Multichannel polarization-controllable superpositions of orbital angular momentum states, Adv. Mater. **29**, 1603838 (2017).

[12] A. M. Yao and M. J. Padgett, Orbital angular momentum: origins, behavior and applications, Adv. Opt. Photonics **3**, 161 (2011).

[13] A. E. Willner, H. Huang, Y. Yan, Y. Ren, N. Ahmed, G. Xie, C. Bao, L. Li, Y. Cao, Z. Zhao, J. Wang, M. P. J. Lavery, M. Tur, S. Ramachandran, A. F. Molisch, N. Ashrafi, and S. Ashrafi, Optical communications using orbital angular momentum beams, Adv. Opt. Photonics **7**, 66 (2015).

[14] A. S. Ostrovsky, C. Rickenstorff-Parrao, and V. Arrizón, Generation of the "perfect" optical vortex using a liquid-crystal spatial light modulator, Opt. Lett. **38**, 534 (2013).

[15] J. García-García, C. Rickenstorff-Parrao, R. Ramos-García, V. Arrizón, and A. S. Ostrovsky, Simple technique for generating the perfect optical vortex, Opt. Lett. **39**, 5305 (2014).

[16] P. Vaity and L. Rusch, Perfect vortex beam: Fourier transformation of a Bessel beam, Opt. Lett. **40**, 597 (2015).

[17] P. Li, Y. Zhang, S. Liu, C. Ma, L. Han, H. Cheng, and J. Zhao, Generation of perfect vectorial vortex beams, Opt. Lett. **41**, 2205 (2016).

[18] J. Yu, C. Zhou, Y. Lu, J. Wu, L. Zhu, and W. Jia, Square lattices of quasi-perfect optical vortices generated by two-dimensional encoding continuous-phase gratings, Opt. Lett. **40**, 2513 (2015).

[19] S. Fu, T. Wang, and C. Gao, Perfect optical vortex array with controllable diffraction order and topological charge, J. Opt. Soc. Am. A **33**, 1836 (2016).

[20] X. Li, H. Ma, C. Yin, J. Tang, H. Li, M. Tang, J. Wang, Y. Tai, X. Li, and Y. Wang, Controllable mode transformation in perfect optical vortices, Opt. Express **26**, 651 (2018).

[21] Y. Liu, Y. Ke, J. Zhou, Y. Liu, H. Luo, S. Wen, and D. Fan, Generation of perfect vortex and vector beams based on Pancharatnam-Berry phase elements, Sci. Rep. **7**, 44096 (2017).

[22] Y. Zhang, W. Liu, J. Gao, and X. Yang, Generating focused 3D perfect vortex beams by plasmonic metasurfaces, Adv. Opt. Mater. **6**, 1701228 (2018).

[23] M. Chen, M. Mazilu, Y. Arita, E. M. Wright, and K. Dholakia, Dynamics of microparticles trapped in a perfect vortex beam, Opt. Lett. **38**, 4919 (2013).

[24] C. Zhang, C. Min, L. Du, and X. C. Yuan, Perfect optical vortex enhanced surface plasmon excitation for plasmonic structured illumination microscopy imaging, Appl. Phys. Lett. **108**, 201601 (2016).

[25] Z. Kuang, W. Perrie, S. P. Edwardson, E. Fearon, and G. Dearden, Ultrafast laser parallel microdrilling using multiple annular beams generated by a spatial light modulator, J. Phys. D **47**, 115501 (2014).

[26] C. Zhou, J. Jia, and L. Liu, Circular Dammann grating, Opt. Lett. **28**, 2174 (2003).

[27] U. Levy, B. Desiatov, I. Goykhman, T. Nachmias, A. Ohayon, and S. E. Meltzer, Design, fabrication, and characterization of circular Dammann gratings based on grayscale lithography, Opt. Lett. **35**, 880 (2010).

[28] H. Dammann and E. Klotz, Coherent optical generation and inspection of two-dimensional periodic structures, Opt. Acta **24**, 505 (1977).

[29] C. Zhou and L. Liu, Numerical study of Dammann array illuminators, Appl. Opt. **34**, 5961 (1995).

[30] P. Chen, S. J. Ge, L. L. Ma, W. Hu, V. Chigrinov, and Y. Q. Lu, Generation of Equal-Energy Orbital Angular Momentum Beams Via Photopatterned Liquid Crystals, Phys. Rev. Appl. **5**, 044009 (2016).

[31] S. Zhao and P. S. Chung, Design of a circular Dammann grating, Opt. Lett. **31**, 2387 (2006).

[32] D. Luo, X. W. Sun, H. T. Dai, and H. V. Demir, Polarization-dependent circular Dammann grating made of azo-dye-doped liquid crystals, Appl. Opt. **50**, 2316 (2011).

[33] X. Wang, S. Wu, W. Yang, C. Yuan, X. Li, Z. Liu, M. Tseng, V. G. Chigrinov, H. Kwok, D. Shen, and Z. Zheng, Light-driven liquid crystal circular Dammann grating fabricated

by a micro-patterned liquid crystal polymer phase mask, Polymers **9**, 380 (2017).

[34] L. Marrucci, C. Manzo, and D. Paparo, Optical Spin-to-Orbital Angular Momentum Conversion in Inhomogeneous Anisotropic Media, Phys. Rev. Lett. **96**, 163905 (2006).

[35] W. Ji, C. H. Lee, P. Chen, W. Hu, Y. Ming, L. Zhang, T. H. Lin, V. Chigrinov, and Y. Q. Lu, Meta-q-plate for complex beam shaping, Sci. Rep. **6**, 25528 (2016).

[36] X. Ling, X. Zhou, K. Huang, Y. Liu, C. W. Qiu, H. Luo, and S. Wen, Recent advances in the spin Hall effect of light, Rep. Prog. Phys. **80**, 066401 (2017).

[37] P. Yeh and C. Gu, *Optics of Liquid Crystal Displays* (John Wiley & Sons, New York, 1999).

[38] M. Schadt, H. Seiberle, and A. Schuster, Optical patterning of multi-domain liquid-crystal displays with wide viewing angles, Nature **381**, 212 (1996).

[39] V. G. Chigrinov, V. M. Kozenkov, and H. S. Kwok, *Photoalignment of Liquid Crystalline Materials: Physics and Applications* (John Wiley & Sons, Chichester, 2008).

[40] V. Chigrinov, S. Pikin, A. Verevochnikov, V. Kozenkov, M. Khazimullin, J. Ho, D. D. Huang, and H. S. Kwok, Diffusion model of photoaligning in azo-dye layers, Phys. Rev. E **69**, 061713 (2004).

[41] P. Chen, L. L. Ma, W. Duan, J. Chen, S. J. Ge, Z. H. Zhu, M. J. Tang, R. Xu, W. Gao, T. Li, W. Hu, and Y. Q. Lu, Digitalizing self-assembled chiral superstructures for optical vortex processing, Adv. Mater. **30**, 1705865 (2018).

[42] J. Kim, Y. Li, M. N. Miskiewicz, C. Oh, M. W. Kudenov, and M. J. Escuti, Fabrication of ideal geometric-phase holograms with arbitrary wavefronts, Optica **2**, 958 (2015).

[43] J. Ni, C. Wang, C. Zhang, Y. Hu, L. Yang, Z. Lao, B. Xu, J. Li, D. Wu, and J. Chu, Three-dimensional chiral microstructures fabricated by structured optical vortices in isotropic material, Light Sci. Appl. **6**, e17011 (2017).

[44] C. Peng, Y. Guo, T. Turiv, M. Jiang, Q. H. Wei, and O. D. Lavrentovich, Patterning of lyotropic chromonic liquid crystals by photoalignment with photonic metamasks, Adv. Mater. **29**, 1606112 (2017).